An overview and comparison of structural form finding methods for general networks

D. Veenendaal *, P. Block

Institute of Technology in Architecture, ETH Zurich, Wolfgang-Pauli-Strasse 15, 8093 Zurich, Switzerland

ARTICLE INFO

ABSTRACT

This paper discusses and compares existing form finding methods for discrete networks. Well-known methods such as the force density method, dynamic relaxation, updated reference strategy and others are discussed by mathematically structuring and presenting them in the same way, using the same notation and combining terminology. Based on this, a single computational framework using a sparse branch-node data structure is presented. It is shown how each method approaches the initial equilibrium problem, defines and linearizes the equilibrium equations applied to linear elements, and uses particular solving strategies. This framework marginalizes any differences related to operating platforms, programming language and style, offering a better baseline for independent comparison of performance and results. As a consequence, it is possible to more clearly relate, distinguish and compare existing methods, allow for hybrid methods and identify new avenues for research.

© 2012 Elsevier Ltd. All rights reserved.

1. Introduction

The principle of *form follows force* is particularly relevant in structures that transfer their loads purely through axial or in-plane forces. In these cases where no bending occurs, shape is determined by forces and vice versa. Examples of discrete structures following this principle include unstrained gridshells (compression), cable-nets (tension) and tensegrity (both). These form-active shapes are not known in advance, and therefore require a *form finding* process. Early examples of form finding using physical models include the hanging chain models by Antoni Gaudí and hanging membranes of Heinz Isler. Since the 1960s, and with the advent of the computer age, research has focused on developing numerical methods, initially applied to the design of cable-net roofs. Despite almost half a century of literature on numerical form finding methods, thorough comparisons remain rare. Subsequently, it is generally unclear to what extent these methods differ and in which cases one may be preferable over another. Compounding this problem is the apparent divide between researchers focusing on particular methods, in spite of them setting similar goals. Comparison is not straightforward as a variety of nomenclatures, mathematical structuring and notation is used. The authors have previously addressed this problem (Veenendaal and Block, 2011), simultaneously with, but independently of Basso and Del Grosso (2011), who focused on recent methods derived from the force density method.

1.1. Objective

The objective of this paper is to compare existing form finding methods for discrete networks and identify key distinctions. In order to achieve this, well-known methods are presented in a single mathematical formulation and implemented in the same computational framework. For this paper, the framework is applied to unloaded, self-stressed networks.

1.2. Outline

An overview will be given of form finding in Section 2, starting with the definition. A categorization and chronology of existing methods for self-stressed networks is presented. Based on literature review and results of this paper, three main families of methods are distinguished. Existing reviews and comparisons found in literature are discussed as a preamble to our own comparison framework. In Section 3, existing, well-known form finding methods are presented in a single notation while combining their respective terminologies, revealing many equivalencies. Seven distinct methods have been identified and implemented in our framework for computational comparison. An overview of key differences between (categories of) methods and a comparative table of equations are provided, subsequently explained in more detail. These differences can be viewed as decisions in our framework to arrive at specific methods. Section 4 discusses three extended approaches from literature for networks with a non-uniform force distribution. Three examples are shown in Section 5: a uniform force network comparing all seven methods; a non-uniform force

---

* Corresponding author. Tel.: +41 0 446332803; fax: +41 0 446331041.
  E-mail addresses: dveenend@ethz.ch (D. Veenendaal), pblock@ethz.ch (P. Block).

network comparing the three extended approaches; and a minimal surface compared to uniform force and force-density networks and to results from the membrane/cable-net analogy.

2. Form finding

Before presenting the framework, a definition of form finding is given (Section 2.1 and a categorization of form finding methods is proposed (Section 2.2). A brief survey of existing reviews (Section 2.3) with a summary of common criticisms (Section 2.4) and and existing comparisons (Section 2.5) are given.

2.1. Definition (s)

The design process by which the shape of form-active structures and systems is determined is widely called either *form finding* or *shape finding*. Adapted from Lewis (2003), the definition of form finding is:

Finding an (optimal) shape of a [form-active structure] that is in (or approximates) a state of static equilibrium.

Such a definition is generally accepted and used, but has been criticized by Haber and Abel (1982) for not acknowledging the fact that in many cases the stresses cannot be imposed and are, like the shape, also unknown. Instead, they suggest calling the problem of form finding the *initial equilibrium problem*. Sensitive to this issue, recent works by Bletzinger et al. (e.g. Dieringer, 2010) typically offer variations of the following, narrower definition of form finding:

Finding a shape of equilibrium of forces in a given boundary with respect to a certain stress state.

Over the past decade, a new notion of form finding has necessitated the distinction between *classical* and *modern* form finding, to acknowledge additional constraints. Some recent definitions of modern form finding are much broader: "finding an appropriate architectural and structural shape" (Coenders and Bosia, 2006), or "a structural optimisation process which uses the nodal coordinates as variables" (Basso and Del Grosso, 2011).

2.2. Methods and categorization

In the last five decades several methods of form finding have been developed (Fig. 1). Earlier methods were typically applied to discrete cable-net structures and extended by later methods to surface elements for membrane structures (denoted by triangles in Fig. 1). It is possible to categorize these in three main families:

- *Stiffness matrix methods* are based on using the standard elastic and geometric stiffness matrices. These methods are among the oldest form finding methods, and are adapted from structural analysis.
- *Geometric stiffness methods* are material independent, with only a geometric stiffness. In several cases, starting with the force density method, the ratio of force to length is a central unit in the mathematics. Several later methods are presented as generalizations or extensions of the force density method (Haber and Abel, 1982; Bletzinger and Ramm, 1999; Pauletti and Pimenta, 2008), independent of element type, often discussing prescription of forces rather than force densities.
- *Dynamic equilibrium methods* solve the problem of dynamic equilibrium to arrive at a steady-state solution, equivalent to the static solution of static equilibrium.

Note that our categorization is similar to recent work by Bletzinger (2011). The category of stiffness matrix methods may

be the least well-defined, with no consensus on name and principal sources. Similar classifications of these methods are (in chronological order): non-linear network computation (Schek, 1974), computer erecting (Linkwitz, 1976), Newton–Raphson iteration (Barnes, 1977), non-linear displacement analysis (Haber and Abel, 1982) and transient stiffness (Lewis, 2003). Each of these classifications refer to at least one reference by Haug et al., published in the period 1970–1972 (e.g. Haug and Powell, 1972), and Argyris, Angelopoulos et al., published in the period 1970–1974 (e.g. Argyris et al., 1974).

The methods in Fig. 1 that first developed a formulation with (triangular) surface elements are applied to discrete networks in this paper. Each of these methods also give the case for discrete cable elements and/or cable-nets (Haber and Abel, 1982; Barnes and Wakefield, 1984; Tabarrok and Qin, 1992; Singer, 1995; Maurin and Motro, 1998; Bletzinger and Ramm, 1999; Pauletti and Pimenta, 2008). The work by Tabarrok and Qin (1992) was applied to examples of cable-reinforced membrane structures instead of cable-nets.

2.3. Existing reviews

Comprehensive reviews of form finding methods can be found (Haber and Abel, 1982; Basso and Del Grosso, 2011; Linkwitz, 1976; Barnes, 1977; Tan, 1989; Meek and Xia, 1999; Nouri-Baranger, 2004; Lewis, 2008; Tibert and Pellegrino, 2003), although different in scope, for example focusing only on tension structures or tensegrity. Several references have become somewhat dated. Some do not offer critical comments and serve purely as non-comparative reviews (Basso and Del Grosso, 2011; Linkwitz, 1976; Meek and Xia, 1999). In other cases, they serve merely as an introduction for a method put forward by the author (s) (Haber and Abel, 1982; Nouri-Baranger, 2004; Lewis, 2008).

2.4. Common criticisms

A summary of existing criticisms found in literature is provided here, by category. These criticisms do not necessarily reflect the opinion of the authors.

Stiffness matrix methods include material properties, which is unnecessary, computationally costly, and may lead to difficulty in control of (stable) convergence (Haber and Abel, 1982; Barnes, 1977; Nouri-Baranger, 2004; Lewis, 2008).

Geometric stiffness methods applied in their linear form, produce results that are not constructionally practicable (Barnes, 1977) and can serve only as a preliminary result. Linear results of the force density method are dependent on mesh density and anisotropy. Additional iterations are necessary (Tan, 1989) for uniform or geodesic networks (Barnes, 1977; Lewis, 2008) or shape dependent loading (Haber and Abel, 1982), making the method non-linear (however, the authors argue that this is inherent to these particular applications and not a disadvantage of the method). Force densities or geometric stiffnesses are not meaningful or intuitive quantities (Haber and Abel, 1982; Tan, 1989; Nouri-Baranger, 2004), making it difficult to predict the outcome for a prescribed set of force densities (the authors note that newer methods often focus on strategies to deal with this, prescribing forces rather than force densities).

Dynamic equilibrium methods require too many parameters, such as the time step, to control stability and convergence (Nouri-Baranger, 2004) (the authors note this can be reduced to a single damping parameter and often to a trivial value for the time step $\Delta t = 1$). The mass and damping parameters are also fictitious, and have no physical representation (Nouri-Baranger, 2004) and may therefore not be meaningful.
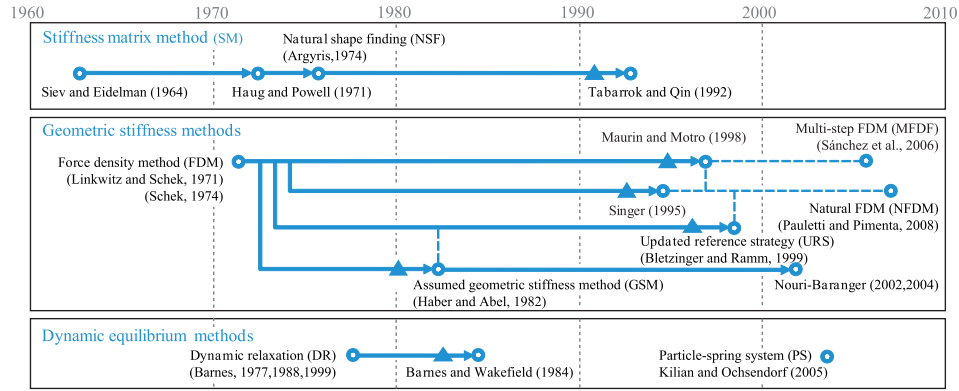
Fig. 1. Development and categorization of form finding methods with key references. Arrows denote descendence, dotted lines denote independent but related methods and triangles a first formulation using surface elements.

2.5. Existing comparisons

There are very few sources that compare the actual performance and results of different methods. Barnes (1977) compared the storage and operation requirements of dynamic relaxation and stiffness matrix methods per iteration and quotes required numbers of iterations, concluding dynamic relaxation to be favourable in the case of cable networks. This was further demonstrated by Lewis (2003, 1989) who compared several configurations of cable nets. The conclusion was that the stiffness matrix method did not converge for one of the examples and that dynamic relaxation had lower total computational cost for examples with many degrees of freedom.

3. Framework

The framework presented here uses a single data structure and mathematical notation, thus exposing key differences between methods. These differences appear as choices within the framework (Fig. 2, Table 1), or in the form of different equations (Table 2).

Following a certain string of choices leads to one of seven particular methods (Table 1). The most fundamental decision is between three apparent ways in which these methods solve the initial equilibrium problem, i.e. the method of *regularization*, described in Section 3.2. Another decision is the type of incremental *formulation*, discussed in Section 3.3.

The rest of Section 3 provides information about the implementation of the framework. Section 3.5 defines static equilibrium and discusses linearization as a first step towards a solution. The core of any implemented method is characterized by the definitions of

Table 1
Methods implemented in this paper, with corresponding choices made in the framework (Fig. 2). Choices in blue denote fundamental approaches in regularization (see Section 3.2). (See below mentioned reference for further information.)

Method	Choices
Stiffness matrix method (**SM**)	1.3.2.1a.1
(Siev and Eidelman, 1964; Haug and Powell, 1972; Argyris et al., 1974; Tabarrok and Qin, 1992)	
Force density method (**FDM**)	1.3.1.1b.0
(Linkwitz and Schek, 1971)	
Multi-step force-density method with force adjustment (**MFDF**)	1.1.1.1b.1
(Sánchez et al., 2007; Maurin and Motro, 1997)	
Geometric stiffness method (**GSM**)	1.1.2a.1b.1
(Haber and Abel, 1982; Bletzinger and Ramm, 1999; Nouri-Baranger, 2002, 2004; Pauletti and Pimenta, 2008)	
Updated reference strategy with homotopy mapping (**URS**HM)	1.2.2a.1.1
(Bletzinger and Ramm, 1999)	
Dynamic relaxation (**DR**)	2.3.2.2a.2
(Barnes, 1988; Barnes, 1999)	
Particle spring system (**PS**)	2.3.2.2b.2
(Kilian and Ochsendorf, 2005)	

force densities $\mathbf{q}$ and the stiffness and/or mass matrices, $\mathbf{K}$ and $\mathbf{M}$, which are provided for each method in Table 2. The equations in Table 2 are explained in more detail as follows: the data structure and discretization of the geometry in Section 3.4; the forces and force densities in Section 3.6 ; and the stiffness and mass in Sections 3.7 and 3.8. Different solving strategies and possible convergence criteria are given in Sections 3.9 and 3.10.

Lists of abbreviations and variables are provided in the Appendices A and B. The mathematical notation in this paper is

Fig. 2. Overview of the framework's critical choices (and Section 3) leading to different methods. Choices in blue denote fundamental approaches in regularization (see Section 3.2). (For interpretation of reference to color in this figure legend, the reader is referred to the web version of this article.)

Table 2
Overview of force densities, global stiffness and mass per method.

Method	$\mathbf{q}$ $[m \times 1]$	Eq.	$\mathbf{K}$ $[n_i \times n_i]$		Eq.	$\mathbf{M}$ $[n_i \times n_i]$	Eq.
SM	$\mathbf{L}^{-1}\mathbf{f}_0 \;+$ $\mathbf{L}^{-1}\mathbf{EA}\epsilon$	(14)	$\mathbf{C}_i^T\mathbf{L}^{-1}\mathbf{FC}_i$	$- \;\; \mathbf{C}_i^T\mathbf{U}^2\mathbf{L}^{-3}\mathbf{FC}_i$ $+ \;\; \mathbf{C}_i^T\mathbf{U}^2\mathbf{L}_0^{-1}\mathbf{EAC}_i$	(23)		
FDM	$\mathbf{q}$		$\mathbf{C}_i^T\mathbf{Q}\mathbf{C}_i$		(26)		
MFDF	$\mathbf{L}_{\mathrm{ref}}^{-1}\mathbf{f}_0$	(17)	$\mathbf{C}_i^T\mathbf{L}_{\mathrm{ref}}^{-1}\mathbf{FC}_i$		(27)		
GSM	$\mathbf{L}_{\mathrm{ref}}^{-1}\mathbf{f}_0$	(17)	$\mathbf{C}_i^T\mathbf{L}_{\mathrm{ref}}^{-1}\mathbf{FC}_i$		(27)		
URS$_\mathrm{HM}$	$\mathbf{L}^{-1}\mathbf{f}_0(\lambda_s) \;+$ $\mathbf{L}_{\mathrm{ref}}^{-1}\mathbf{f}_0(1-\lambda_s)$	(18)	$\mathbf{C}_i^T\mathbf{L}^{-1}\mathbf{FC}_i(\lambda_s)$ $\mathbf{C}_i^T\mathbf{L}_{\mathrm{ref}}^{-1}\mathbf{FC}_i(1-\lambda_s)$	$- \;\; \mathbf{C}_i^T\mathbf{U}^2\mathbf{L}^{-3}\mathbf{FC}_i(\lambda_s)$	(25)		
DR	$\mathbf{L}^{-1}\mathbf{f}_0 \;+$ $\mathbf{L}^{-1}\mathbf{EA}\epsilon$	(14)				$\delta_{ij}\mathbf{C}_i^T\mathbf{L}^{-1}\mathbf{FC}_i$ $\delta_{ij}\mathbf{C}_i^T\mathbf{L}_0^{-1}\mathbf{EAC}_i$	(28)
PS	$\mathbf{L}^{-1}\mathbf{f}_0 \;+$ $\mathbf{L}^{-1}(\mathbf{L}-\mathbf{L}_0)\mathbf{k}_s \;+$ $\mathbf{L}^{-1}\mathbf{C}_i\mathbf{V}_{t-\Delta t/2}\mathbf{U}\mathbf{L}^{-1}\mathbf{k}_d$	(15)	$\mathbf{C}_i^T\mathbf{L}^{-1}\mathbf{FC}_i$	$- \;\; \mathbf{C}_i^T\mathbf{U}^2\mathbf{L}^{-3}\mathbf{FC}_i$ $+ \;\; \mathbf{C}_i^T\mathbf{U}^2\mathbf{L}^{-2}k_s\mathbf{C}_i$		$\mathbf{M}$	

as follows: italics represent scalars, bold lower-case letters represent vectors and bold upper-case letters represent matrices. An upper-case version of a letter denoting a vector is the diagonal matrix of that vector.

3.1. Implemented methods

Seven distinct methods have been implemented which apply to the form finding of networks of cables, rods or bars. Table 1 lists each of these methods and corresponding key references. The table also shows choices in our framework necessary to arrive at that particular method.

Note that the authors concluded that the references for SM are largely equivalent. Haug-Powell's method (Haug and Powell, 1972) is a 3D extension of Siev–Eidelman's, or grid method (Siev and Eidelman, 1964), and natural shape finding (NSF) (Argyris et al., 1974) originally operated by displacing supports from a flat state.

The references for GSM have also been concluded to be conceptually equivalent methods: assumed geometric stiffness method (GSM) (Haber and Abel, 1982; Nouri-Baranger, 2002, 2004), updated reference strategy (URS) (Bletzinger and Ramm, 1999) and the natural force density method (NFDM) (Pauletti and Pimenta, 2008).

3.2. Regularization

The problem of form finding, expressed as a purely geometrical problem "is singular with respect to tangential shape variations" (Bletzinger and Ramm, 1999). This means that, for example, in the axis of a minimal-length cable nothing governs the position of intermediate nodes and no unique solution exists unless some method of *regularization* is used. There are three ways to solve the initial equilibrium problem (appearing in blue in Fig. 2 and Table 1), also discussed by Bletzinger (2011):

1. materialize the problem by adding elastic stiffness;
2. solve for forces in the (updated) reference configuration; or
3. solve for the analogous, dynamic steady-state solution with diagonal mass (and damping) matrices.

3.3. Formulation

There are two common incremental formulations for non-linear, large displacement analysis, the *Total Lagrangian Formulation* (TLF) and the *Updated Lagrangian Formulation* (ULF). They determine how the forces and stiffnesses at each increment are calculated. These formulations are applied in form finding methods. URS offers a mixed formulation of the two, called *homotopy mapping* (HM).

In TLF the variables are referred to the initial configuration Γ_0, whereas in ULF they are referred to a *reference* configuration Γ_{ref}, updated in each step from the last calculated *actual*, or *viable* configuration Γ. Fig. 3 visualizes the three formulations. HM introduces factor λ_s which determines, for each step, how the forces, referred to the (updated) reference configuration and the actual configuration, are interpolated. This approach results in an inner and outer loop, with inherently different convergence criteria.

The following observations are made:

• Existing stiffness matrix and dynamic equilibrium methods use TLF.
• Force density and geometric stiffness methods in linear form use TLF. In non-linear form they use ULF.
• URS has a unique mixed formulation, HM, which reverts to ULF if all λ_s are zero.

In this paper SM is also combined with ULF, which stabilizes the method. Furthermore, for URS$_\mathrm{HM}$, the reference configuration was updated at each iteration (not just each step), removing the inner loops, which improved overall convergence speed.

3.4. Data structure and discretization

Throughout our framework, regardless of the form finding method, a branch-node matrix $\mathbf{C}$ is used to describe the topology of a network Γ of bars and nodes (Schek, 1974; Fenves and Branin Jr., 1963).

Note that the transpose of $\mathbf{C}$ is defined as the incidence matrix in graph theory (Bondy and Murty, 1976), and the incidence matrix in turn has been compared to standard approaches in the finite element method to assemble stiffness matrices (Christensen, 1988).

For a network with m branches and n nodes in three-dimensional space a $[3m \times 3n]$ branch-node matrix is constructed (Linkwitz, 1999):

$$\mathbf{C} = \begin{bmatrix} \bar{\mathbf{C}} & & \\ & \bar{\mathbf{C}} & \\ & & \bar{\mathbf{C}} \end{bmatrix} \tag{1}$$

where the entries of the ith row and jth column of the $[m \times n]$ submatrix $\bar{\mathbf{C}}$ are:

$$\bar{C}_{ij} = \begin{cases} +1 & \text{if node } j \text{ is the head of branch } i \\ -1 & \text{if node } j \text{ is the tail of branch } i \\ 0 & \text{otherwise} \end{cases}$$

Note that the direction of the branch vectors may be chosen arbitrarily. Furthermore, the use of three submatrices $\bar{\mathbf{C}}$, one for each
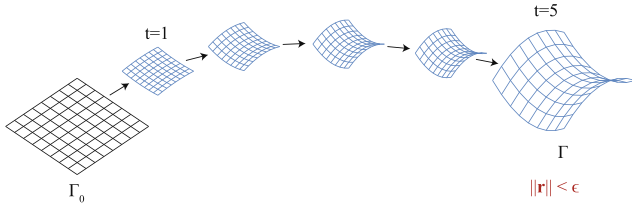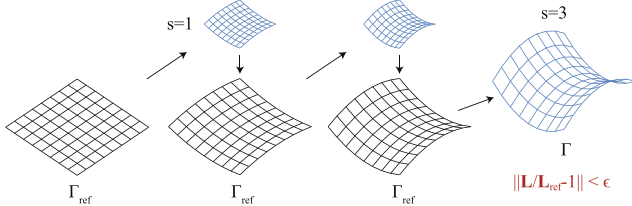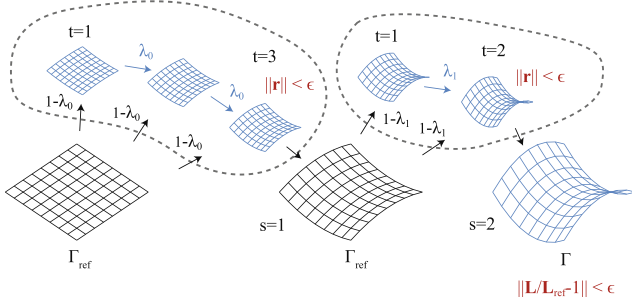
Fig. 3. Total and Updated Lagrangian Formulations, and Homotopy Mapping, with iterations *t* and steps *s*, and corresponding convergence criteria in red. (For interpretation of reference to color in this figure legend, the reader is referred to the web version of this article.)

dimension, is done for later convenience, to avoid triple equations or equations with triple terms.

The [$3n \times 1$] nodal coordinate vector $\mathbf{x}$ is:

$$\mathbf{x} = \begin{bmatrix} \bar{\mathbf{x}} \\ \bar{\mathbf{y}} \\ \bar{\mathbf{z}} \end{bmatrix} = \begin{cases} \bar{\mathbf{x}} = (x_1, x_2, \ldots, x_n)^{\mathrm{T}} \\ \bar{\mathbf{y}} = (y_1, y_2, \ldots, y_n)^{\mathrm{T}} \\ \bar{\mathbf{z}} = (z_1, z_2, \ldots, z_n)^{\mathrm{T}} \end{cases} \tag{2}$$

where $\bar{\mathbf{x}}, \bar{\mathbf{y}}$ and $\bar{\mathbf{z}}$ are vectors containing *n* coordinates in Cartesian directions. For later application, the *n* nodes are declared to be either interior (i.e. free) or fixed nodes. Note that this may differ in each direction if, for example, a node is fixed in *x* direction but free to move in *y* direction. In our case, the nodes are assumed to be either interior or fixed in all directions, with $n = n_i + n_f$. The $3n$ columns of the branch-node matrix $\mathbf{C}$ and the $3n$ rows of the nodal coordinate vector $\mathbf{x}$ are resequenced accordingly:

$$\mathbf{C} = \begin{bmatrix} \mathbf{C}_i & \mathbf{C}_f \end{bmatrix} \tag{3}$$

where $\mathbf{C}_i$ is a [$3m \times 3n_i$] branch-node matrix for the interior nodes and $\mathbf{C}_f$ is a [$3m \times 3n_f$] branch-node matrix for the fixed nodes.

$$\mathbf{x} = \begin{bmatrix} \mathbf{x}_i \\ \mathbf{x}_f \end{bmatrix} \tag{4}$$

where $\mathbf{x}_i$ is a [$3n_i \times 1$] coordinate vector of the interior nodes and $\mathbf{x}_f$ is a [$3n_f \times 1$] vector of the fixed nodes. The coordinate difference vector $\mathbf{u}$ can be written as a function of $\mathbf{C}$ and the coordinate vector $\mathbf{x}$:

$$\mathbf{u} = \begin{bmatrix} \bar{\mathbf{u}} \\ \bar{\mathbf{v}} \\ \bar{\mathbf{w}} \end{bmatrix} = \mathbf{C}\mathbf{x} \tag{5}$$

where $\bar{\mathbf{u}}, \bar{\mathbf{v}}$ and $\bar{\mathbf{w}}$ are vectors, each containing *m* coordinate differences in corresponding Cartesian direction. With $\mathbf{U}, \bar{\mathbf{U}}, \bar{\mathbf{V}}$ and $\bar{\mathbf{W}}$, the diagonal matrices of $\mathbf{u}, \bar{\mathbf{u}}, \bar{\mathbf{v}}$ and $\bar{\mathbf{w}}$, the branch lengths $\mathbf{L}$ are:

$$\mathbf{L} = \begin{bmatrix} \bar{\mathbf{L}} & & \\ & \bar{\mathbf{L}} & \\ & & \bar{\mathbf{L}} \end{bmatrix} \tag{6}$$

with

$$\bar{\mathbf{L}} = (\bar{\mathbf{U}}^2 + \bar{\mathbf{V}}^2 + \bar{\mathbf{W}}^2)^{\frac{1}{2}}$$

3.5. Equilibrium and linearization

In this Section the equilibrium of the network and linearization is discussed, characterized by three new quantities: force densities $\mathbf{q}$, stiffness matrix $\mathbf{K}$ and mass matrix $\mathbf{M}$. Their definition for different methods is discussed in subsequent Sections 3.6, 3.7 and 3.8, and summarized in Table 2.

The network is in a state of equilibrium if the sum of the external loads $\mathbf{p}$ and internal forces at all nodes is zero. Writing the internal forces in terms of the branch forces $\mathbf{g}$ as a function of coordinate differences $\mathbf{u}$ we obtain (Linkwitz, 1999):

$$\mathbf{p} - \mathbf{C}_i^{\mathrm{T}}\mathbf{g}(\mathbf{u}) = \mathbf{0} \tag{7}$$

Typically this system of non-linear equilibrium equations is solved by linearization with a first order Taylor expansion, i.e. Newton's method, with respect to change in position $\mathbf{x}, \Delta\mathbf{x}$ (Linkwitz, 1999):

$$\mathbf{C}_i^{\mathrm{T}}\mathbf{J}_{\mathbf{g}}(\mathbf{x})\Delta\mathbf{x} = \mathbf{p} - \mathbf{C}_i^{\mathrm{T}}\mathbf{g}(\mathbf{u}) \tag{8}$$

where $\mathbf{J}_{\mathbf{g}}(\mathbf{x})$ is the Jacobian of the branch forces $\mathbf{g}$ with respect to the nodal coordinates $\mathbf{x}$. By convention the resulting LHS matrix and RHS vector in Eq. (8) are called the stiffness matrix $\mathbf{K}$ (see for each method Table 2) and and the (residual) force vector $\mathbf{r}$:

$$\mathbf{K}\Delta\mathbf{x} = \mathbf{r} \tag{9}$$

which is commonly known as Hooke's Law.

Note that deriving this equilibrium equation from the principles of virtual work and minimum total potential energy has been shown in general (Haber and Abel, 1982; Bletzinger and Ramm, 1999) and specifically for bar elements (Bletzinger and Ramm, 1999; Tabarrok and Qin, 1992). These sources show subsequent linearization as well, but this has also been specifically explained with the use of the branch-node matrix $\mathbf{C}$ (Singer, 1995; Linkwitz, 1999).

When considered as a dynamic problem, Eq. (7) can also be linearized with a first order Taylor expansion, with respect to change in velocity $\mathbf{v}, \Delta\mathbf{v}$, over time interval Δt:

$$\mathbf{C}_i^{\mathrm{T}}\frac{dt}{d}\left(\mathbf{J}_{\mathbf{g}}(\mathbf{v})\right)\frac{\Delta\mathbf{v}}{\Delta t} = \mathbf{p} - \mathbf{C}_i^{\mathrm{T}}\mathbf{g}(\mathbf{u}) \tag{10}$$

where $\mathbf{J}_{\mathbf{g}}(\mathbf{v})$ is the Jacobian of the branch forces $\mathbf{g}$ with respect to the nodal velocities $\mathbf{v}$. The LHS matrix is the mass matrix $\mathbf{M}$ (see for each method Table 2):

$$\mathbf{M}\frac{\Delta\mathbf{v}}{\Delta t} = \mathbf{r} \tag{11}$$

which is commonly known as Newton's Second Law.

This paper focuses on unloaded, self-stressed networks, so the external load vector $\mathbf{p} = \mathbf{0}$. The *m* element forces $\mathbf{f}$ are decomposed into the forces $\mathbf{g}(\mathbf{u})$ in each direction using the direction vector, or *direction cosines* $\mathbf{UL}^{-1}$ (sometimes expressed in angles).

$$\mathbf{g}(\mathbf{u}) = \mathbf{UL}^{-1}\mathbf{f} \tag{12}$$

Using Eqs. (5), (8) and (12), and with $\mathbf{p} = \mathbf{0}$, the n_i nodal residual forces $\mathbf{r}$ are:

$$\mathbf{r} = -\mathbf{C}_i^T\mathbf{UL}^{-1}\mathbf{f} = -\mathbf{C}_i^T\mathbf{L}^{-1}\mathbf{FCx} \tag{13}$$

in which the ratios $\mathbf{L}^{-1}\mathbf{f}$ are commonly known as force densities $\mathbf{q}$ (Schek, 1974), or tension coefficients (Barnes, 1977).

3.6. Forces and force densities

The forces in a network of elastic bars are determined by an initial stress and an elastic term. Written as force-to-length ratios, i.e. force densities or tension coefficients:

$$\mathbf{q} = \mathbf{L}^{-1}\mathbf{f} = \mathbf{q}_g + \mathbf{q}_e = \mathbf{L}^{-1}\mathbf{f}_0 + \mathbf{L}^{-1}\mathbf{EA}\varepsilon \tag{14}$$

where prescribed forces $\mathbf{f}_0 = \mathbf{A}\sigma_0$ and strains $\varepsilon = \mathbf{L}_0^{-1}(\mathbf{l} - \mathbf{l}_0)$. The first term $\mathbf{q}_g$ is a function of initial (Cauchy) stresses σ_0, cross-sections $\mathbf{A}$ and actual lengths $\mathbf{L}$. The second term $\mathbf{q}_e$ is a function of elasticities or Young's moduli $\mathbf{E}$, cross-sections $\mathbf{A}$, strains ε, actual lengths vector $\mathbf{l}$ and the initial lengths, or rest lengths, $\mathbf{L}_0$, or as a vector $\mathbf{l}_0$.

The bar can also be modelled as a spring, in which case spring constants $\mathbf{k}_s$ are equivalent to the diagonal of $\mathbf{L}_0^{-1}\mathbf{EA}$ and damping forces are introduced as well. According to Baraff and Witkin (1998), "the damping force should depend on the component of the system's velocity". The damping force in the springs is calculated from the nodal velocities $\mathbf{v}$ using the branch-node matrix $\mathbf{C}_i$ and decomposed using the direction cosines $\mathbf{UL}^{-1}$. The force densities for springs are:

$$\mathbf{q} = \mathbf{L}^{-1}\mathbf{f}_0 + \mathbf{L}^{-1}(\mathbf{L} - \mathbf{L}_0)\mathbf{k}_s + \mathbf{L}^{-2}\mathbf{C}_i\mathbf{V}_{t-\Delta t/2}\mathbf{Uk}_d \tag{15}$$

where $\mathbf{k}_d$ are damping constants and $\mathbf{v}_{t-\Delta t/2}$ the nodal velocities at time $t - \Delta t/2$. The first term has been added here by the authors to apply PS to constant force networks. Note also that for *zero-length* springs, the second term reduces to constant force densities of value $\mathbf{k}_s$. The third term vanishes as a steady-state is approached.

For the geometric stiffness methods, material independence is assumed (see Section 3.6.1) and only the first term in Eq. 14 remains:

$$\mathbf{q} = \mathbf{q}_g = \mathbf{L}^{-1}\mathbf{f}_0 \tag{16}$$

One can prescribe either forces or force densities. In linear FDM the force densities $\mathbf{q}$ are simply prescribed constants, often a trivial value, e.g. $\mathbf{q} = \mathbf{1}$. In non-linear form, the reference configuration is updated at each step s. The resulting *modified* force density $\mathbf{q}_{mod}$, using the updated reference lengths $\mathbf{L}_{ref}$, is then:

$$\mathbf{q} = \mathbf{q}_{mod} = \mathbf{L}_{ref}^{-1}\mathbf{f}_0 \tag{17}$$

When using HM, one effectively interpolates between Eqs. (16) and (17). The force density $\mathbf{q}$ at each (inner) iteration t is:

$$\mathbf{q} = \lambda_s\mathbf{q}_g + (1 - \lambda_s)\mathbf{q}_{mod} \tag{18}$$

The factor $\lambda_s = 0$ for the first (outer) step, then usually increasing rapidly towards the original problem with a factor $\lambda_s = 0.9$ for later steps (Bletzinger and Ramm, 1999). If $\lambda_s = 0$ for each step, i.e. using only the modified problem, the method is equivalent to GSM.

Regardless of the definition of the force densities, whether constant or otherwise, the residual force vector $\mathbf{r}$ of the entire network can be calculated using Eq. (13).

The force densities for each method are shown in the first column of Table 2.

3.6.1. Material independence

The problem of form finding is in principle a geometric one, and thus material independent. Indeed, Argyris et al. (1974) do acknowledge that "it is possible to develop a shape finding method [...] which does not consider the elastic properties of the structure". Tabarrok and Qin (1992) assume that for form finding "the membrane has a very small Young's modulus". For GSM, Haber and Abel (1982) confirm that any value for E is acceptable, but for simplicity is set to zero. Similarly, for DR, Barnes (1999) prescribes only a constant tension and no elasticity when searching for geodesic networks.

There is an important consequence of material independence. After convergence, the m initial lengths $\mathbf{L}_0$ can be (re-) calculated based on m desired forces $\mathbf{f}$ (Argyris et al., 1974), and/or the m desired stiffnesses $\mathbf{EA}$, without disturbing the state of equilibrium (Gründig et al., 2000):

$$\mathbf{L}_0 = \mathbf{L}(\mathbf{EA}^{-1}\mathbf{F} + \mathbf{I}^{-1})^{-1} \tag{19}$$

where $\mathbf{I}$ is an identity matrix.

3.6.2. Comparison of MFDF and GSM

MFDF was recently proposed (Sánchez et al., 2007), but its central premise was already given by Maurin and Motro (1997). The force densities are updated at each step s based on the updated geometry Γ_{ref}:

$$\mathbf{q}_{s+1} = \mathbf{Q}_s\mathbf{F}_s^{-1}\mathbf{f}_0 = \mathbf{L}_{ref}^{-1}\mathbf{F}_{ref}\mathbf{F}_{ref}^{-1}\mathbf{f}_0 = \mathbf{L}_{ref}^{-1}\mathbf{f}_0 \tag{20}$$

GSM considers the problem from a continuum mechanical point of view:

$$\mathbf{q}_{mod} = \mathbf{L}_{ref}^{-1}\mathbf{As}_0 = \mathbf{L}_{ref}^{-1}\mathbf{A}\sigma_0 = \mathbf{L}_{ref}^{-1}\mathbf{f}_0 \tag{21}$$

The forces $\mathbf{f}_0$ are prescribed as a function of 2nd Piola–Kirchhoff stresses $\mathbf{s}_0$ in the reference configuration instead of Cauchy stresses σ_0 of the actual configuration. GSM assumes these two stresses to be equivalent at each step. This assumption is valid when converging to a state of equilibrium, where both configurations and thus both stresses become identical.

After rewriting, Eq. (20) is identical to Eq. (21) per iteration. The distinction is that MFDF starts from prescribed force densities $\mathbf{q}_0$ as input whereas GSM from prescribed forces $\mathbf{f}_0$ and initial lengths $\mathbf{L}_0$. Of course, these initial values influence convergence, depending on which start closer to the final solution.

3.7. Stiffness

The stiffness of a bar element is typically decomposed in two terms: a geometric stiffness $\mathbf{K}_g$ and an elastic stiffness $\mathbf{K}_e$ (Haug and Powell, 1972; Knudson and Scordelis, 1972; Argyris et al., 1974). The former describes the bar's resistance to lateral loading, and the latter the elongation of the bar under load. Using the branch-node formulation, the stiffnesses are:

$$\mathbf{K} = \mathbf{K}_g + \mathbf{K}_e \tag{22}$$

where,

$$\mathbf{K}_g = \mathbf{C}_i^T\mathbf{L}^{-1}\mathbf{FC}_i - \mathbf{C}_i^T\mathbf{U}^2\mathbf{L}^{-2}\mathbf{L}^{-1}\mathbf{FC}_i \tag{23a}$$

$$\mathbf{K}_e = \mathbf{C}_i^T\mathbf{U}^2\mathbf{L}^{-2}\mathbf{L}_0^{-1}\mathbf{EAC}_i \tag{23b}$$

The bar can also be modelled as a spring where $\mathbf{L}_0^{-1}\mathbf{EA1} = \mathbf{k}_s$ and $\mathbf{L}^{-1}\mathbf{f} = \mathbf{L}^{-1}(\mathbf{L} - \mathbf{L}_0)\mathbf{k}_s$ (see Table 2).

With Eq. (14) and $\mathbf{f}_0 = \mathbf{0}$, it is possible to rewrite Eq. (23):

$$\mathbf{K}_g = \mathbf{C}_i^T\mathbf{L}^{-1}\mathbf{FC}_i \tag{24a}$$

$$\mathbf{K}_e = \mathbf{C}_i^T\mathbf{U}^2\mathbf{L}^{-2}\mathbf{L}^{-1}\mathbf{EAC}_i \tag{24b}$$

This solution has been previously derived in branch-node formulation by Linkwitz (1999). Setting each elasticity $E = 0$, the geometric stiffness remains, which written in the reference configuration is:

$$\mathbf{K} = \mathbf{K}_{\mathrm{mod}} = \mathbf{C}_i^{\mathrm{T}} \mathbf{L}_{\mathrm{ref}}^{-1} \mathbf{F} \mathbf{C}_i \tag{25}$$

Replacing the force densities with constant values leads to the original formulation of FDM:

$$\mathbf{K} = \mathbf{C}_i^{\mathrm{T}} \mathbf{Q} \mathbf{C}_i \tag{26}$$

When applying HM, Eqs. (23a) and (25) are interpolated:

$$\mathbf{K} = \lambda_s \mathbf{K}_g + (1 - \lambda_s) \mathbf{K}_{\mathrm{mod}} \tag{27}$$

The stiffness matrices for each method are shown in the second column of Table 2.

3.8. Mass

DR uses *lumped nodal masses*, derived from the element stiffnesses. From Eqs. (9) and (11) we can see that within a time interval Δt, it is indeed possible to relate the concepts of mass and stifness. DR defines the masses as the greatest possible, direct stiffness for each node, to deal with large displacements during form finding (Barnes and Wakefield, 1984; Barnes, 1999):

$$\mathbf{M} = \frac{\Delta t^2}{2} \delta_{ij} (\mathbf{C}_i^{\mathrm{T}} \mathbf{L}^{-1} \mathbf{F} \mathbf{C}_i + \mathbf{C}_i^{\mathrm{T}} \mathbf{L}_0^{-1} \mathbf{EA} \mathbf{C}_i) \tag{28}$$

$$\text{where} \quad \delta_{ij} = \begin{cases} 1 & \text{if} \quad i = j \\ 0 & \text{if} \quad i \neq j \end{cases}$$

A computationally more efficient implementation for Eq. (28) is:

$$\mathbf{m} = \frac{\Delta t^2}{2} |\mathbf{C}_i^{\mathrm{T}}| (\mathbf{L}^{-1} \mathbf{F} + \mathbf{L}_0^{-1} \mathbf{EA}) \mathbf{1} \tag{29}$$

Because the resulting masses are diagonal matrices, or vectors, DR has been called a vector-based method. The benefit of this is that inverting the diagonal $\mathbf{M}$ to solve for $\Delta \mathbf{v}$ is significantly easier and faster than inverting a non-diagonal stiffness matrix $\mathbf{K}$ to solve for $\Delta \mathbf{x}$. Interestingly, Barnes (1999) does not draw a firm conclusion on whether conventional stiffness matrices or lumped masses offer the greatest benefit for convergence.

In PS, the masses $\mathbf{M}$ are simply prescribed.

The mass matrices for each method are shown in the third column of Table 2.

3.9. Converging to equilibrium

For non-linear, iterative methods, using Eq. (9), a common solving procedure at each iteration is:

$$\mathbf{x}_{i,t+1} = \mathbf{x}_{i,t} + \Delta \mathbf{x}_{i,t} \tag{30a}$$

$$\mathbf{x}_{i,t+1} = \mathbf{x}_{i,t} + \mathbf{K}^{-1} \mathbf{r} \tag{30b}$$

In linear FDM, the force densities are set as constant values $\mathbf{q}$. So, using Eqs. (13) and (26), Eq. (30b) can be rewritten and solved directly (Schek, 1974):

$$\mathbf{x}_{i,t+1} = \mathbf{x}_{i,t} + \mathbf{D}_i^{-1}(-\mathbf{D}_i \mathbf{x}_{i,t} - \mathbf{D}_f \mathbf{x}_f) \tag{31a}$$

$$\mathbf{x}_{i,t+1} = \mathbf{D}_i^{-1}(-\mathbf{D}_f \mathbf{x}_f) \tag{31b}$$

where $\mathbf{D}_i = \mathbf{C}_i^{\mathrm{T}} \mathbf{Q} \mathbf{C}_i$ and $\mathbf{D}_f = \mathbf{C}_i^{\mathrm{T}} \mathbf{Q} \mathbf{C}_f$. Note that the solution is independent of the initial coordinates $\mathbf{x}_{i,t}$.

Stating the problem as dynamic equilibrium, using Eq. (11), we obtain the following iteration at time t in centred finite difference form (Barnes, 1999) for DR:

$$\mathbf{v}_{t+\Delta t/2} = \mathbf{v}_{t-\Delta t/2} + \Delta \mathbf{v}_t \tag{32a}$$

$$\mathbf{v}_{t+\Delta t/2} = \mathbf{v}_{t-\Delta t/2} + \Delta t \mathbf{M}^{-1} \mathbf{r} \tag{32b}$$

$$\mathbf{x}_{i,t+\Delta t} = \mathbf{x}_{i,t} + \Delta t \mathbf{v}_{t+\Delta t/2} \tag{32c}$$

where Δt is the time step. Note the similarity in form between Eqs. (30) and (32). The solving procedure in DR is also known as Leapfrog integration, and is analogous to (Velocity) Verlet integration. Damping is introduced by either viscous damping (Barnes, 1988) (controlled by one parameter) or kinetic damping (Barnes, 1999) (automatic). In PS, a typical implementation uses either explicit classic 4th order Runge–Kutta (RK4) or implicit Backward Euler (BE). The procedure for RK4 replaces (32b):

$$\mathbf{k}(t, \mathbf{x}_i) = \mathbf{M}^{-1} \mathbf{r}(t, \mathbf{x}_i) \tag{33a}$$

$$\mathbf{k}_1 = \Delta t \mathbf{k}(t, \mathbf{x}_{i,t}) \tag{33b}$$

$$\mathbf{k}_2 = \Delta t \mathbf{k}\left(t + \frac{1}{2}\Delta t, \mathbf{x}_{i,t} + \frac{1}{2}\mathbf{k}_1\right) \tag{33c}$$

$$\mathbf{k}_3 = \Delta t \mathbf{k}\left(t + \frac{1}{2}\Delta t, \mathbf{x}_{i,t} + \frac{1}{2}\mathbf{k}_2\right) \tag{33d}$$

$$\mathbf{k}_4 = \Delta t \mathbf{k}(t + \Delta t, \mathbf{x}_{i,t} + \mathbf{k}_3) \tag{33e}$$

$$\mathbf{v}_{t+\Delta t/2} = \mathbf{v}_{t-\Delta t/2} + \frac{1}{6}(\mathbf{k}_1 + 2\mathbf{k}_2 + 2\mathbf{k}_3 + \mathbf{k}_4) \tag{33f}$$

For BE, the procedure derived by Baraff and Witkin (1998) includes the stiffness matrix $\mathbf{K}$ and a Jacobian matrix of the damping forces with respect to velocities, $\mathbf{J}(\mathbf{v})$:

$$\mathbf{J}(\mathbf{v}) = -k_d \mathbf{C}_i \tag{34}$$

Damping occurs through the damping forces (Eq. (15)) controlled by damping coefficient k_d, and through a drag coefficient b. Prior to Eq. (32c), the procedure is:

$$\mathbf{B} \Delta \mathbf{v}_t = \mathbf{c} \tag{35a}$$

$$\mathbf{B} = \mathbf{M} - \Delta t \mathbf{C}_i^{\mathrm{T}} \mathbf{J}(\mathbf{v}) - \Delta t^2 \mathbf{K} \tag{35b}$$

$$\mathbf{c} = \Delta t(\mathbf{r} + \Delta t \mathbf{K} \mathbf{v}_{t-\Delta t/2}) \tag{35c}$$

$$\mathbf{v}_{t+\Delta t/2} = \mathbf{v}_{t-\Delta t/2} + \mathbf{B}^{-1}(\mathbf{c} - b\mathbf{v}_{t-\Delta t/2}) \tag{35d}$$

To solve the linear system of equations at each iteration in all of these methods, Cholesky decomposition has been used in this paper. Several sources apply some form of the Conjugate Gradient method Brakke, 1992; Baraff and Witkin, 1998; Maurin and Motro, 2001, and GSM discusses Jacobi and Gauss–Seidel's method (Haber and Abel, 1982).

3.10. Convergence criteria

To determine convergence, the authors mention the following options, where the first three are adapted from Lewis (2003):

1. small values of residual forces ($||\mathbf{r}|| < \epsilon$);
2. small variations in the displacements between successive iterations ($||\mathbf{x}_{t+1} - \mathbf{x}_t|| < \epsilon$);
3. small variations in the total length of the bars, between successive iterations ($||\mathbf{l} - \mathbf{l}_{\mathrm{ref}}|| < \epsilon$);
4. small values of the normal strain ($||\mathbf{L}_{\mathrm{ref}}^{-1} \mathbf{l} - \mathbf{1}|| < \epsilon$), or
5. small values of the kinetic energy ($||\frac{1}{2}\mathbf{V}^2 \mathbf{m}|| < \epsilon$), and/or
6. maximum number of iterations, steps ($t < t_{\max}, s < s_{\max}$) or duration of computational time reached.

Note that criteria 2–5 can each be expressed as a function of the change in position $||\Delta \mathbf{x}||$. This paper uses criteria 1 and/or 4 depending on the formulation with tolerance $\epsilon = 1e^{-3}$, and criterion 6 for specific cases. Example 1 (see Section 5.1) also uses the total length of the elements as a criterion to compare when methods achieve the same level of accuracy.

4. Non-uniform forces and force densities

In Section 3.6 it became clear that form finding typically requires either the presciption of forces or force densities in a network to obtain the shape in equilibrium. Without prior experience in form finding, a straightforward approach would then be to prescribe a trivial value (e.g. **1**) for either forces **f** or force densities **q**. Schek's two theorems (Schek, 1974) state that the resulting shapes correspond respectively to (I) unloaded nets with a minimal sum of lengths and (II) unloaded nets with a minimal sum of squared lengths (weighted by **q**), illustrated by Maurin and Motro (1997).

However, resulting networks may be impractical, requiring force distributions that are unknown and not straightforward to prescribe. In this Section, methods to obtain shapes with either non-uniform force, or force density distributions are discussed. This is possible by including additional geometrical constraints in an optimzation problem (see Section 4.1), by reintroducing elasticity (see Section 4.2), or by providing geometrical control over deformation during form finding (see Sections 4.3 and 4.4).

4.1. Constrained problems

In cases where additional constraints are known, a minimization problem may be formulated subject to those constraints. Optimization then determines the required stress state. Often some or all information is known about the required shape. Several examples employ a non-linear least squares method: cable-nets constrained by fixed (initial) lengths (Schek, 1974), feasible tensegrity structures (Zhang and Ohsaki, 2006) or target surfaces for cable-nets (Knudson and Scordelis, 1972; Ohyama and Kawamata, 1972; Arcaro and Klinka, 2009; Van Mele and Block, 2011). The last two references, for example, use Gauss–Newton algorithm and the more advanced Levenberg–Marquardt algorithm, respectively.

4.2. Elastic control

In the case of a geometry with prescribed initial lengths $\mathbf{L}_0$, Barnes (1999) suggests in DR to prescribe real stiffnesses **EA** for the interior branches with force density controlled boundaries. This is also the case for SM with TLF, effectively turning the form finding method into an analysis method. DR's use of elasticity is analogous to prescribing spring constants $\mathbf{k}_s$ and rest lengths $\mathbf{L}_0$ in PS.

4.3. Control strings

For high point membranes, peak stresses may occur at the top, due to increasing radial stresses. Similarly, stresses towards the top of cable-nets may increase or decrease depending on the mesh layout. To automatically grade membrane stresses along the radial lines, Barnes (1999) describes *control strings*, which "govern [...] the plane of the surface but have no effect normal to the surface". The strings are force density controlled and their out-of-plane component, normal to the surface, is suppressed. This method has been applied to a discrete network in Section 5.2.

4.4. Element size control

URS introduces *element size control* to adapt surface stresses automatically during form finding if an isotropic stress state is not possible (Wüchner and Bletzinger, 2005; Linhard, 2009). Stresses are altered once a critical deformation is reached. The method is presented in the context of membranes and is adapted to line

elements for this paper. The upper and lower bound of the allowable deformation is controlled by a single parameter α_{max} with respect to an initial or a *maximum allowable* configuration. The deformation is tracked using the determinant of the deformation gradient, α, at each iteration, which for line elements simplifies to:

$$\alpha = \mathbf{L}_{max}^{-1}\mathbf{l} \tag{36}$$

In this case, the prescribed forces **f** are then scaled depending on the deformation. For each branch i, where $i = 1, \ldots, m$:

$$f_{i,s+1} = f_{i,s}\frac{\alpha_i}{\hat{\alpha}_i} \tag{37}$$

where,

$$\hat{\alpha}_i = \begin{cases} \alpha_{max} & \text{if } \alpha_i > \alpha_{max} \\ 1/\alpha_{max} & \text{if } \alpha_i < 1/\alpha_{max} \\ \alpha_i & \text{otherwise} \end{cases} \tag{38}$$

However, oscillatory or even divergent behaviour has been reported when using element size control, though the user can limit the number of form finding steps to just a few (Linhard, 2009). This is because in original URS each step produces a viable configuration and after only a few steps the result is likely to be satisfactory. Indeed, one linear GSM or URS step may prove sufficient.

5. Examples

The framework presented here is applied to three examples. The first is a saddle-shape minimal-length net, to compare the performance of several form finding methods when prescribing constant forces. The second is a high-point net, where constant forces are no longer possible, and previous methods do not apply directly. The resulting shape and forces from three possible approaches are compared. In the third and last example a minimal surface (Scherk's first surface) is compared to a minimal-length (constant force) net and a minimal squared length (constant force density) net.

5.1. Example 1: Saddle

To compare the performance of different methods, a saddle shape with constant forces **f** = **1** and fixed boundaries is sought. The dimensions in are 10×10 with a height of 5 (Fig. 4).

Two version of DR have been tested, one with viscous damping DR_{vis} (Barnes, 1988), one with kinetic damping DR_{kin} (Barnes, 1999). Three versions of PS were tested, one with viscous damping and RK4, $PS_{RK4,vis}$, one with spring damping and RK4, PS_{RK4} and one with spring damping and BE, PS_{BE}. For DR, for each element the stiffness $EA = 0$. For PS parameters k_s, k_d and b were all set to 0.5. Time step $\Delta t = 1$, except for PS_{RK4} where $\Delta t = 0.2$ (changed to avoid instability) and masses **m** = **1**, except $PS_{RK4,vis}$ where **m** = **2** (changed to avoid instability).

Table 3 shows the time and iterations required to solve the problem, for increasing degrees of freedom (dof's). Note that the resulting durations have been normalized with respect to the minimum solving time, $t_{norm} = \frac{t_{mean}}{t_{min}}$.

These results were obtained after an initial calculation was performed with a fixed tolerance $\epsilon = 1e^{-3}$ for their respective convergence criteria (Fig. 3). The largest sum of lengths $\Sigma\mathbf{L}$ was then taken as an entirely new convergence criterium in order to objectively compare the convergence of the methods for a result of equal accuracy. Each method was executed 100 times and these results were averaged. The standard deviation of all results consistently ranged between 9% and 11%.

Fig. 5 shows the computational time needed depending on the degrees of freedom (dof's), plotted on a log–log scale. Appearing
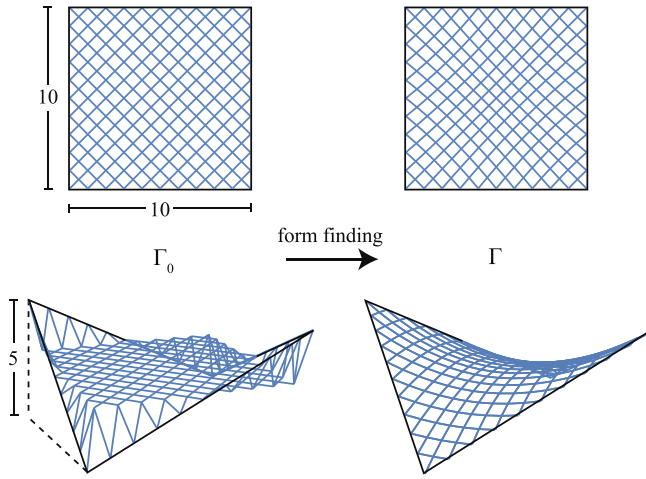
Fig. 4. Form finding of saddle with 543 dof's.

Table 3
Normalized duration t_{norm} of form finding and number of iterations (t), best result in **bold**.

dof's	75	183	339	543
SM	1.25 (**8**)	N/A	N/A	N/A
SM$_{ULF}$	1.44 (13)	4.22 (16)	6.26 (18)	9.93 (17)
MFDF	**1.00** (14)	**1.00** (16)	**1.00** (18)	**1.00** (17)
GSM	1.52 (16)	2.64 (15)	3.77 (14)	3.73 (13)
URS$_{HM}$	1.38 (10)	3.13 (**8**)	4.31 (**9**)	5.36 (**8**)
DR$_{vis}$	1.22 (**8**)	5.40 (34)	15.54 (63)	24.66 (96)
DR$_{kin}$	1.41 (16)	5.19 (32)	10.36 (42)	13.16 (16)
PS$_{RK4,vis}$	1.78 (17)	3.68 (22)	6.74 (28)	11.30 (50)
PS$_{RK4}$	4.10 (39)	6.58 (39)	13.57 (60)	22.73 (67)
PS$_{BE}$	6.31 (37)	11.30 (32)	14.44 (30)	20.33 (30)
t_{min} [s]	0.007	0.015	0.026	0.040
ΣL [m]	117.66	176.16	235.11	293.47

and ULF, the adapted method SM$_{ULF}$ showed polynomial growth $O(n^c)$ as well. Surprisingly, it is superior to DR in this case and requires a roughly constant number of iterations. PS with either explicit RK4 or implicit BE did not show fast convergence overall, but these methods were developed for cloth animation, which has more constraints, and allows shear and bending behaviour. From Fig. 5 it can be seen that the latter does start overtaking other dynamic methods at higher dof's. This is consistent with Baraff and Witkin (1998) who report implicit solvers to be faster than explicit ones, based on examples with at least 2602 nodes (presumably 7806 dof's).

Based on these results, MFDF would seem to be the fastest method for the form finding of minimal-length nets in this range of dof's. As noted in Section 3.6, its advantage is explained by the fact that it automatically starts with one force density-controlled iteration before becoming force-controlled. The other methods start directly from the prescribed forces meaning they are dependent on the initial geometry, in our case a flat net (Fig. 4). Notice the nearly constant number of iterations for the geometry and/or updated reference based methods SM$_{ULF}$, MFDF, GSM and URS$_{HM}$, but also the implicit dynamic PS$_{BE}$. URS$_{HM}$ exhibits the lowest number of iterations needed. This suggests that for implementations with high cost per iteration (e.g. with higher order elements), URS$_{HM}$ could potentially be faster than GSM and MFDF within this range of dof's, especially when starting with a force density controlled-iteration.

5.2. Example 2: High point

For a high-point net, the forces are no longer constant and vary towards the top. If constant forces are imposed throughout the network, elements tend to deform such that no practical solution is found. This means that the methods from the previous example, each based on prescribed forces, become impractical as well. To cope with this situation, several approaches have been discussed (see Section 4). In this example, three approaches in which the deformation of the elements is controlled are discussed: the simple case of FDM with orthotropic force densities; orthotropic forces using control strings (see Section 4.3); and orthotropic forces applying element size control (see Section 4.4). In these examples, $\mathbf{t}$ is the ratio of radial forces to tangential forces $\mathbf{t} = \mathbf{F}_0^{-1}\mathbf{f}_{0,rad}$, or the radial to tangential force densities $\mathbf{t} = \mathbf{Q}_0^{-1}\mathbf{q}_{0,rad}$.

The initial geometry of this example is a cone, cut off at the top. The top radius of the cone is 2, the bottom is 10 and it has a height of 5. The top and bottom edges form fixed boundaries.

Fig. 6 shows typical results of FDM. In the example on the right, the force density is twice as high in the radial links as the

as lines, the required time for all methods seems to exhibit polynomial growth $O(n^c)$ with $c > 0$. MFDF is even approximately linearly dependent on the dof's.

For SM, the standard method did not converge for 183 dof's and above (see Table 3), which agrees with Lewis (1989), who noted that "for a structure with 189 degrees of freedom, any realistic limits of computer time would have been exceeded, unless steps to treat the numerical ill-conditioning are taken" and that without doing so, SM "shows a strong exponential relationship [$O(c^n)$] between the CPU time and the size of the problem considered". However, after introducing an elasticity $EA = 1$ for each element
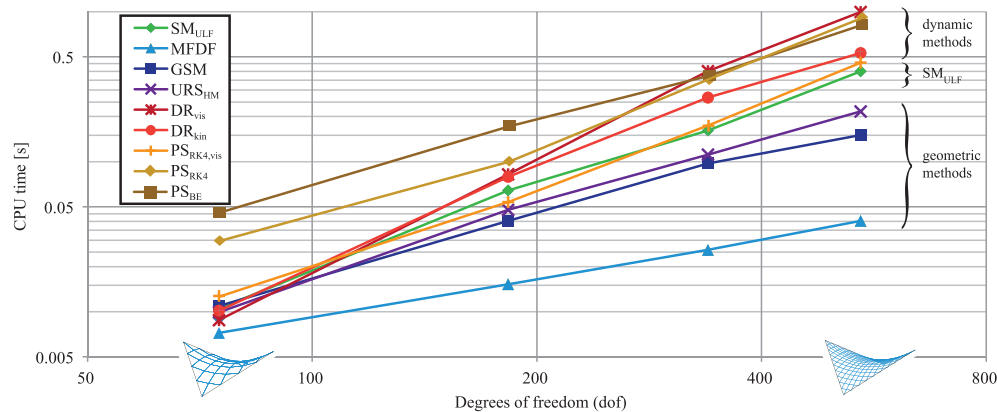

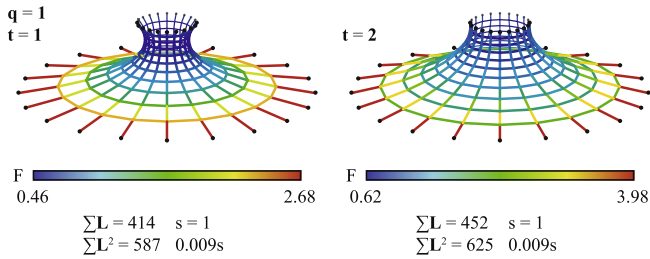**Fig. 5.** Comparison of the efficiency of methods.

Fig. 6. FDM with force density ratios **t** = **1** or **t** = **2**.

tangential links. Observe that both radial and tangential link forces decrease smoothly towards the top.

In Fig. 7 control strings are present along the radial direction. A practical value of the control string force density is $\mathbf{q}_{cs} = \mathbf{F}_0\mathbf{t}$. In these results, the tangential forces remain as prescribed, so the same value throughout. By combining GSM (or URS with $\lambda_s = 0$) with element size control (see Section 4.4), the results from Fig. 8 are obtained. The maximum allowable configuration is chosen to be the actual configuration from the first linear step. The top two examples in Fig. 8 converged after three steps for sufficiently small normal strain $\|\mathbf{L}_{ref}^{-1}\mathbf{l} - \mathbf{1}\| < \epsilon$, where $\epsilon = 1e^{-3}$. The bottom two examples in Fig. 8 are obtained after prescribing five steps ($s_{max} = 5$) and feature a more evenly spaced mesh. The force distribution seems to fall in between the extremes offered by FDM and DR with control strings, as the tangential link forces range from nearly equal after three steps to graded after five steps.

From these results, it is clear that the force distribution and therefore shape obtained depends on the method. Therefore, whether one result is preferable depends entirely on the user and the context of the problem.

In terms of the numerical approach, it is noted that DR with control strings requires a large amount of iterations to converge.

GSM with element size control exhibited oscillatory behaviour for values $\alpha_{max} \neq 1$ in Eq. (37), similar to that reported by Linhard (2009). In those cases, the prescribed forces are only altered outside a certain range of allowable deformation. An additional relaxation parameter (Linhard, 2009) led to eventual, but slow convergence and impractical force distributions. Instead, if $\alpha_{max} = 1$ as in Fig. 8, the prescribed force is always recalculated.

The numerical drawbacks observed in the latter two methods seem to indicate why commercial applications often simply rely on linear solutions. This suggests that there is room to develop a more stable and robust control method in the future, in which the user can more freely explore this range of equally feasible solutions.

5.3. Example 3a: Scherk's first surface

This example is used to compare constant force and constant force density networks to a minimal surface. The drawbacks of
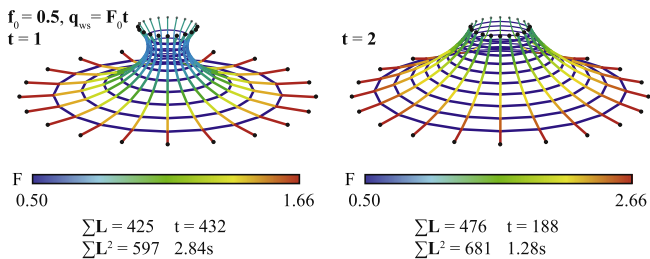

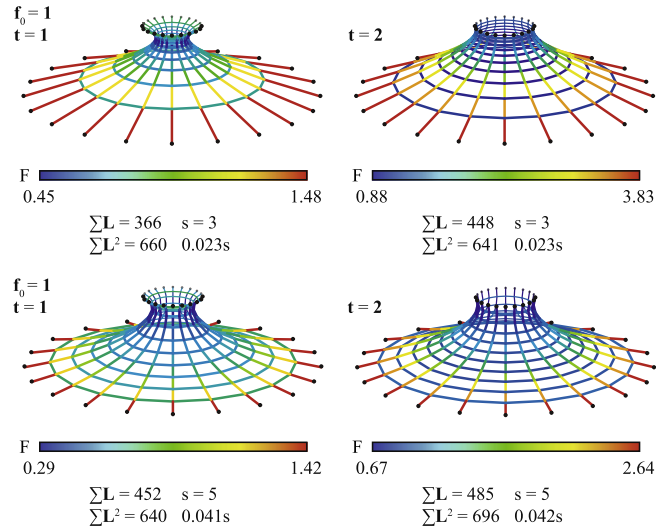**Fig. 7.** DR$_{vis}$ with control strings and force ratios **t** = **1** or **t** = **2**.

Fig. 8. GSM with element size control, force ratios **t = 1** or **t = 2**, with 3 or 5 steps and $\alpha_{max} = 1$.

the membrane analogy used to relate a surface to a network are also discussed. A minimal surface is often the basis for the design of tensile structures. Fig. 9a–c show the results of a comparison between:

- a minimal-length net with $\mathbf{f}_0 = \mathbf{1}$ (min. $\Sigma\mathbf{L}$) using MFDF;
- a minimal squared length net with $\mathbf{q} = \mathbf{1}$ (min. $\Sigma\mathbf{L}^2$) using FDM;
- a network following the minimal surface (Scherk's surface) (min. $\Sigma\mathbf{A}$).

The same topology and boundary conditions are used. The initial geometry is a network with a square orthogonal grid in plan of $\pi \times \pi$. The minimal-length net implodes and does not properly converge, so for Fig. 9a the number of iterations was fixed at 20. The FDM solution in 9b shows a similar grading of forces as the previous example of FDM (Fig. 6). The network in Fig. 9c is obtained by projecting the initial geometry onto the Scherk's surface. The height field, providing the coordinates, is:

$$z(x,y) = \frac{1}{a} \log\left(\frac{\cos ax}{\cos ay}\right) \tag{39}$$

with $a = 0.98$. The resulting required lengths $\mathbf{L}_{ref}$ are then used to calculate force densities at each step:

$$\mathbf{q}_{s+1} = \mathbf{L}_{ref}^{-1}\mathbf{L}\mathbf{q}_s \tag{40}$$

Fig. 9a–c demonstrate that both shape and force distribution of the three networks are not the same. Thus, care is required when using any form finding method for a particular application or towards a particular desired outcome (see also Section 4).

5.4. Example 3b: Membrane and cable-net analogy

The result from Section 5.3 begs the question whether networks can be used to properly model surfaces and surface stresses. In fact, the *cable-net analogy*, deriving stresses from branch forces, has a long tradition in the engineering of tensioned membrane structures (Ströbel, 1995; Gründig et al., 2000). Here, the branch forces **f** are treated as local resultant forces using the local average mesh width, or representative width, thus obtaining surface stresses. Fig. 9d demonstrates the force distribution found through the inverse membrane analogy (Buchholdt et al., 1968) with uniform surface stress.
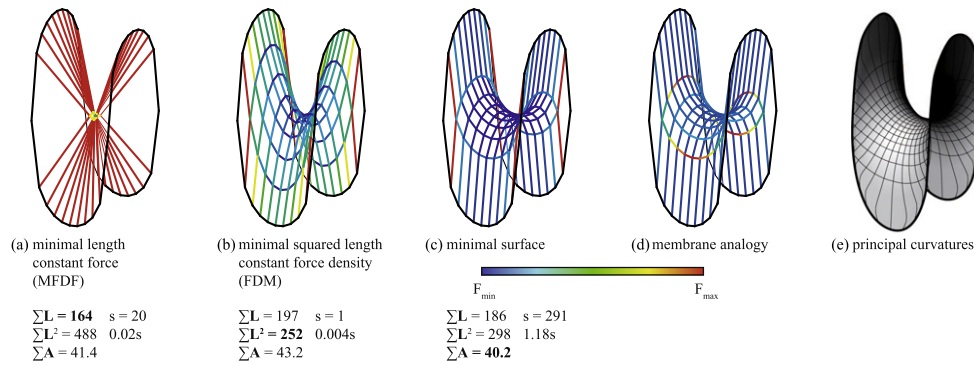
(a) minimal length constant force (MFDF)	(b) minimal squared length constant force density (FDM)	(c) minimal surface	(d) membrane analogy	(e) principal curvatures
$\sum L = \mathbf{164}$ s = 20 $\sum L^2 = 488$ 0.02s $\sum A = 41.4$	$\sum L = 197$ s = 1 $\sum L^2 = \mathbf{252}$ 0.004s $\sum A = 43.2$	$\sum L = 186$ s = 291 $\sum L^2 = 298$ 1.18s $\sum A = \mathbf{40.2}$		

Fig. 9. Minimal-length net (a), minimal squared length net (b) and minimal Scherk's surface (c) with the same boundary conditions. Incorrect forces obtained from the membrane analogy (d) compared with lines of principal curvature (e) as an indicator for an optimal analogous mesh.

When comparing to Fig. 9c to 9d the forces obtained differ. Therefore, the analogy fails to correctly model the surface.

Because the cable-net cannot model the shear stresses of a membrane (Maurin and Motro, 1998), it is only capable of modelling an isotropic surface stress if the cables follow lines of principal curvature. In that case the normal stresses coincide with the principal stresses (no shear). Indeed, the cable-net analogy, though common enough in practice, has been criticized because of its dependence on the mesh density and topology, as well as producing a "stress state in the fabric [...] that is not based on established theoretical calculation" (Nouri-Baranger, 2004).

So, to properly model the surface, the topology should adapt such that the link elements approximately follow these principal curvatures (Fig. 9e). Alternatively, one could simply use surface elements instead of bar elements.

6. Conclusions

The unifying framework presented in this paper allows for and demonstrates the direct comparison of a wide range of different form finding methods. By presenting methods in the same manner and carrying out an extensive review of literature, the following specific observations were made:

- Key differences and similarities between (categories of) methods have been identified (see Fig. 2).
- Methods that use elastic stiffness matrices do not differ fundamentally from one another, and it is acceptable to view them as a single method, as has been done in the past under varying names. Specific features, unique to particular references, are mentioned in Section 3.
- Methods purely based on geometric stiffness, such as GSM, URS (with $\lambda_s = 0$), MFDF and NFDM are largely identical.
- MFDF's central premise (Eq. (20)) was already proposed by Maurin and Motro (1997).
- MFDF's advantage (in our examples) is explained as a starting from an FDM solution, independent of the initial configuration.

Through the examples in Section 5 some additional insights were possible:

- For the form finding of minimal-length nets, MFDF is the most efficient numerical method to apply (of the methods and examples that were compared). Overall, geometric methods are superior to elastic stiffness and dynamic methods.
- For the form finding of nets with non-uniform forces, one can apply FDM or extend the other methods. This leads to a wide range of equally feasible shapes. Because no unique solution

exists, none of these methods are superior per se. If information on the initial geometry is available, elasticity can be involved to find the corresponding unique static solution. If additional geometric constraints for the final geometry are known, optimization methods can be applied.

- For the form finding of networks following minimal surfaces, the cable-net analogy cannot be applied in a straightforward manner.

More generally, the framework provides for three functions:

Didactic instrument: The use of a single type of mathematical formulation provides insight in how each method fundamentally solves the initial equilibrium problem and which parameters are used to control the calculations. In particular, the use of matrix algebra and application to simple, unloaded and self-stressed networks provides an easily reproducible description of these methods. In this way, the framework can also act as a stepping stone, either between literature on methods that are traditionally viewed as vastly different, or towards methods that are commonly seen as difficult to grasp. It may lead to greater understanding and appreciation of such methods, and emphasize their particular contributions. In a similar fashion, the framework offers a basis for extension to more complex element types, material models and solvers, which is the direction of the authors' future work.

Objective comparison and choice: The choice between methods is generally not straightforward, due to the lack of objective, comprehensive reviews and comparisons. By structuring and presenting methods using the same discretization and branch-node data structure, differences related to mathematical notation, operating platforms, programming language and style are marginalized. This offers a better baseline for independent comparison of performance and results, enabling one to make more informed decisions when choosing between methods.

Development of new and hybrid methods: By examining the relation between methods and how they solve the initial equilibrium problem, it may occur to the reader where new possibilities lie for future development of new approaches. The framework allows hybrid solutions combining strengths of existing methods. This potential is already demonstrated by three examples: combining the stiffness matrix methods (SM) with an updated Lagrangian formulation (ULF) for greater stability, updating the reference configuration at each iteration (not just each step) in the updated reference strategy (URS_HM) for more competitive convergence, and combining the particle-spring system (PS) with viscous damping. As shown, some independent but largely identical developments occurred, sometimes decades apart. This framework may avoid such needless repetition and allow future research to be directed towards entirely new discoveries.

Acknowledgements

Appendix A. List of abbreviations

BE	backward Euler method
DR	dynamic relaxation
FDM	force density method
GSM	assumed geometric stiffness method
HM	homotopy mapping
kin	kinetic damping
MFDF	multi-step force-density method with force adjustment
NFDM	natural force density method
NSF	natural shape finding
PS	particle spring system
RK4	classic 4th-order Runge Kutta method
SM	stiffness matrix method
TLF	total Lagrangian formulation
ULF	updated Lagrangian formulation
URS	updated reference strategy
vis	viscous damping

Appendix B. List of variables

Variables in both lower- and upper-case denote vectors and their corresponding diagonal matrices.

$\mathbf{0}$	null vector
$\mathbf{1}$	ones vector
$\mathbf{2}$	vector with two for each entry
α	allowable deformation parameter
Γ	network in actual configuration
Γ_i	network in initial configuration
Γ_{ref}	network in reference configuration
δ	Kronecker delta
Δt	change in time t, or time step
$\Delta \mathbf{v}$	changes in velocity $\mathbf{v}$
$\Delta \mathbf{x}$	changes in position $\mathbf{x}$
ε	Cauchy strains
ϵ	convergence tolerance
λ_s	homotopy factor at step s
σ_0	initial Cauchy stresses
$\mathbf{a}, \mathbf{A}$	cross-sectional areas
b	drag coefficient
$\mathbf{C}$	$[3m \times 3n]$ branch-node matrix
$\mathbf{C}_f$	$[3m \times 3n_f]$ branch-node matrix for fixed nodes
$\mathbf{C}_i$	$[3m \times 3n_i]$ branch-node matrix for interior/free nodes

$\bar{\mathbf{C}}$	$[m \times n]$ branch-node matrix for a network
$\mathbf{D}_i$	$[3n_i \times 3n_i]$ matrix $\mathbf{C}_i^T \mathbf{Q} \mathbf{C}_i$
$\mathbf{D}_f$	$[3n_i \times 3n_f]$ matrix $\mathbf{C}_i^T \mathbf{Q} \mathbf{C}_f$
$\mathbf{E}$	Young's moduli
$\mathbf{f}, \mathbf{F}$	actual branch forces
$\mathbf{f}_0, \mathbf{F}_0$	initial/prescribed branch forces
$\mathbf{f}_{ref}, \mathbf{F}_{ref}$	reference branch forces
$\mathbf{g}(\mathbf{u})$	branch forces decomposed in three-dimensions
$\mathbf{I}$	identity matrix
$\mathbf{J}_i(\mathbf{j})$	Jacobian matrix of a function $\mathbf{i}$ with respect to a vector $\mathbf{j}$
$\mathbf{k}$	increment vector for RK4 as a function of t and $\mathbf{x}_i$
$k_d, \mathbf{k}_d$	damping constant (s)
$k_s, \mathbf{k}_s$	spring constant (s)
$\mathbf{K}$	stiffness matrix
$\mathbf{K}_e$	elastic stiffness matrix
$\mathbf{K}_g$	geometric stiffness matrix
$\mathbf{K}_{mod}$	modified stiffness matrix
$\mathbf{l}, \mathbf{L}$	actual branch lengths
$\mathbf{l}_0, \mathbf{L}_0$	initial branch lengths
$\mathbf{l}_{ref}, \mathbf{L}_{ref}$	reference branch lengths
$\bar{\mathbf{l}}, \bar{\mathbf{L}}$	branch lengths
m	number of branches or springs
$\mathbf{m}, \mathbf{M}$	nodal masses
n, n_f, n_i	number of all, fixed and interior/free nodes
$\mathbf{p}$	external loads
$\mathbf{q}, \mathbf{Q}$	force densities
$\mathbf{q}_e$	elastic force densities
$\mathbf{q}_g$	geometric force densities
$\mathbf{q}_{mod}$	modified force densities
$\mathbf{r}$	residual forces
s	step
$\mathbf{s}_0$	initial/prescribed 2nd Piola–Kirchhoff stresses
t	time or iteration
$\mathbf{t}$	ratios of radial to tangential forces or force densities
$\mathbf{u}, \mathbf{U}$	coordinate differences
$\bar{\mathbf{u}}, \bar{\mathbf{U}}$	coordinate differences in x-direction
$\mathbf{v}, \mathbf{V}$	velocities
$\bar{\mathbf{v}}, \bar{\mathbf{V}}$	coordinate differences in y-direction
$\bar{\mathbf{w}}, \bar{\mathbf{W}}$	coordinate differences in z-direction
x, y, z	coordinate in x-,y-, and z-direction
$\mathbf{x}$	coordinates of all nodes
$\mathbf{x}_f$	coordinates of fixed nodes
$\mathbf{x}_i$	coordinates of interior/free nodes
$\bar{\mathbf{x}}, \bar{\mathbf{y}}, \bar{\mathbf{z}}$	coordinates in x-,y-, and z-direction

References

Arcaro, K.K., Klinka, V.F., 2009. Finite element analysis for geometric shape minimization. Journal of the International Association for Shell and Spatial Structures 50, 79–86.

Argyris, J.H., Angelopoulos, T., Bichat, B., 1974. A general method for the shape finding of lightweight tension structures. Computer Methods in Applied Mechanics and Engineering 3, 135–149.

Baraff, D., Witkin, A., 1998. Large steps in cloth animation. In: SIGGRAPH 98 Computer Graphics Proceedings, Orlando, FL, USA.

Barnes, M.R., 1977. Form-finding and analysis of tension space structures by dynamic relaxation, Ph.D. thesis, City University London, United Kingdom.

Barnes, M., Wakefield, D., 1984. Dynamic relaxation applied to interactive form finding and analysis of air-supported structures. In: Proceedings of Conference on the Design of Air-supported Structures, pp. 147–161.

Barnes, M.R., 1988. Form-finding and analysis of prestressed nets and membranes. Computers and Structures 30, 685–695.

Barnes, M.R., 1999. Form finding and analysis of tension structures by dynamic relaxation. International Journal of Space Structures 14, 89–104.

Basso, P., Del Grosso, A., 2011. Form-finding methods for structural frameworks: a review. In: Proceedings of the International Association of Shells and Spatial Structures, London.

Bletzinger, K.-U., Ramm, E., 1999. A general finite element approach to the form finding of tensile structures by the updated reference strategy. International Journal of Space Structures 14, 131–145.

Bletzinger, K.-U., 2011. Section 12.2: Form finding and morphogenesis. In: I. Munga, J.F. Abel (Eds.), Fifty Years of Progress for Shell and Spatial Structures, Multi-Science, pp. 459–482.

Bondy, J.A., Murty, U.S.R., 1976. Graph Theory with Applications. Elsevier Science Publishing Co., New York.

Brakke, K.A., 1992. The surface evolver. Experimental Mathematics 1, 141–165.

Buchholdt, H.A., Davies, M., Hussey, M.J.L., 1968. The analysis of cable nets. Journal of the Institute of Mathematics and Its Applications 4, 339–358.

Christensen, R., 1988. Network formulation of the finite element method. International Journal of General Systems 14, 59–75.

Coenders, J., Bosia, D., 2006. Computational tools for design and engineering of complex geometrical structures: From a theoretical and a practical point of view. In: Oosterhuis, K., Feireiss, L. (Eds.), Game Set And Match II. On Computer Games, Advanced Geometries, and Digital Technologies. Episode Publishers, p. 006.

Dieringer, F., Carat++ public wiki, 2010.

Fenves, S.J., Branin Jr., F.H., 1963. Network-topological formulation of structural analysis. Journal of the Structural Division, Proceedings of the American Society of Civil Engineers, 483–514.

Gründig, L., Moncrieff, E., Singer, P., Ströbel, D., 2000. A history of the principal developments and applications of the force density method in Germany 1970–1999. In: Proceedings of IASS-IACM 2000 Fourth International Colloquium on Computation of Shell & Spatial Structures, Chania-Crete, Greece.

Haber, R.B., Abel, J.F., 1982. Initial equilibrium solution methods for cable reinforced membranes. Part I – Formulations. Computer Methods in Applied Mechanics and Engineering 30, 263–284.

Haug, E., Powell, G.H., 1972. Analytical shape finding for cable nets. In: Proceedings of the 1971 IASS Pacific Symposium Part II on Tension Structures and Space Frames, 1–5, Tokyo and Kyoto, Japan, pp. 83–92.

Kilian, A., Ochsendorf, J., 2005. Particle-spring systems for structural form finding. Journal of the International Association for Shell and Spatial Structures: IASS 46, 77–84.

Knudson, W.C., Scordelis, A.C., 1972. Cable forces for desired shapes in cable-net structures. In: Proceedings of the 1971 IASS Pacific Symposium Part II on Tension Structures and Space Frames, 1–6, Tokyo and Kyoto, Japan, pp. 93–102.

Lewis, W.J., 1989. The efficiency of numerical methods for the analysis of prestressed nets and pin-jointed frame structures. Computers and Structures 33, 791–800.

Lewis, W.J., 2008. Computational form-finding methods for fabric structures. Proceedings of the ICE – Engineering and Computational Mechanics 161, 139–149.

Lewis, W.J., 2003. Tension structures. Form and Behaviour. Thomas Telford, London, 2003.

Linhard, J., 2009. Numerisch-mechanische Betrachtung des Entwurfsprozesses von Membrantragwerken, Ph.D. thesis, Technische Universität München, Germany, 2009.

Linkwitz, K., Schek, H.J., 1971. Einige Bemerkungen zur Berechnung von vorgespannten Seilnetzkonstruktionen. Ingenieur Archiv 40, 145–158.

Linkwitz, K., 1976. Combined use of computation techniques and models for the process of form finding for prestressed nets, grid shells and membranes. In: Proceedings of Internationalen Symposium Weitgespannte Flächentragwerke.

Linkwitz, K., 1999. Formfinding by the "direct approach" and pertinent strategies for the conceptual design of prestressed and hanging structures. International Journal of Space Structures 14, 73–87.

Maurin, B., Motro, R., 1997. Investigation of minimal forms with density methods. Journal of the International Association for Shell and Spatial Structures 38, 143–154.

Maurin, B., Motro, R., 1998. The surface stress density method as a form-finding tool for tensile membranes. Engineering Structures 20, 712–719.

Maurin, B., Motro, R., 2001. Investigation of minimal forms with conjugate gradient method. International Journal of Solids and Structures 38, 2387–2399.

Meek, J.L., Xia, X., 1999. Computer shape finding of form structures. International Journal of Space Structures 14, 35–55.

Nouri-Baranger, T., 2002. Form finding method of tensile structures. Revised geometric stiffness method. Journal of the International Association for Shell and Spatial Structures 43 (138), 13–21.

Nouri-Baranger, T., 2004. Computational methods for tension-loaded structures. Archives of Computational Methods in Engineering 11, 143–186.

Ohyama, H., Kawamata, S., 1972. A problem of surface design for prestressed cable nets. In: Proceedings of the 1971 IASS Pacific Symposium Part II on Tension Structures and Space Frames, 1–7, Tokyo and Kyoto, Japan, pp. 103–115.

Pauletti, R.M.O., Pimenta, P.M., 2008. The natural force density method for the shape finding of taut structures. Computer Methods in Applied Mechanics and Engineering 197, 4419–4428.

Sánchez, J., Serna, M.Á., Paz, M., 2007. A multi-step force-density method and surface-fitting approach for the preliminary shape design of tensile structures. Engineering Structures 29, 1966–1976.

Schek, H.-J., 1974. The force density method for form finding and computation of general networks. Computer Methods in Applied Mechanics and Engineering 3, 115–134.

Siev, A., Eidelman, J., 1964. Stress analysis of prestressed suspended roofs, Journal of the Structural Division,. Proceedings of the American Society of Civil Engineers, 103–121.

Singer, P., 1995. Die Berechnung von Minimalflächen, Seifenblasen, Membrane und Pneus aus geodätischer Sicht, Ph.D. thesis, University of Stuttgart, Germany, 1995.

Ströbel, D., 1995. Die Anwendung der Ausgleichungsrechnung auf elastomechanische Systeme, Ph.D. thesis, University of Stuttgart, Germany.

Tabarrok, B., Qin, Z., 1992. Nonlinear analysis of tension structures. Computers and Structures 45, 973–984.

Tan, K.Y., 1989. The Computer Design of Tensile Membrane Structures, Ph.D. thesis, University of Queensland, Brisbane, Australia.

Tibert, A.G., Pellegrino, S., 2003. Review of form-finding methods for tensegrity structures. International Journal of Space Structures 18, 209–223.

Van Mele, T., Block, P., 2011. Novel form finding method for fabric formwork for concrete shells. Journal of the International Association of Shell and Spatial Structures 52, 217–224.

Veenendaal, D., Block, P., 2011. A framework for comparing form finding methods. In: Proceedings of the International Association of Shells and Spatial Structures, London.

Wüchner, R., Bletzinger, K.-U., 2005. Stress-adapted numerical form finding of pre-stressed surfaces by the updated reference strategy. International Journal for Numerical Methods in Engineering 64, 143–166.

Zhang, J.Y., Ohsaki, M., 2006. Adaptive force density method for form-finding problem of tensegrity structures. International Journal of Solids and Structures 43, 5658–5673.